Journal of Constructional Steel Research 115 (2015) 303–315

Contents lists available at ScienceDirect

Journal of Constructional Steel Research

Axial tensile behavior and strength of welds for CHS branches to SHS chord joints

Wei Wang [a,b,*], Qing Gu [b], Xinxu Ma [b], Junjie Wang [b]

[a] State Key Laboratory of Disaster Reduction in Civil Engineering, Tongji University, Shanghai 200092, China
[b] Department of Structural Engineering, Tongji University, Shanghai 200092, China

ARTICLE INFO

Article history:
Received 27 December 2014
Received in revised form 23 August 2015
Accepted 28 August 2015
Available online 14 September 2015

Keywords:
Steel tubular joints
Welded joints
Heat affected zone
Strain distribution
Effective length
Axial tensile strength

ABSTRACT

In this work, experimental investigations were conducted on the axial tensile behavior of welds connecting tubular X-joints with CHS branches to a SHS chord. Five non-rigid and three rigid welded joints were tested under monotonic loading conditions. The weld properties were specially measured using a negative mold. Next, the strain distribution, the failure modes and the strength of the welds were obtained. The results indicate that an uneven strain distribution exists in the non-rigid joints in contrast to the uniform strain distribution in the rigid joints. The strength of welds for the non-rigid joints exhibits a significant reduction compared with rigid joints. Finally a predictive formula for the axial tensile strength of the welds is proposed according to the method of effective length based on experimental research and finite element analysis, which is capable of meeting the reliability requirements of the AISC specification.

© 2015 Elsevier Ltd. All rights reserved.

1. Introduction

Single-layer reticulated shells have become a particularly popular choice for large-span roof systems used in steel structures due to their light weight, appealing architectural appearance and ability to be rapidly constructed. Tubular sections are a common selection for the primary load-carrying members of this type of onshore structure. During practical applications, the sections are profiled and welded to form unstiffened X-joints (as shown in Fig. 1 for a typical engineering application). Research has been conducted to examine the behavior of un-stiffened joints, including tubular joint rigidity [1], the flexural behavior of tubular joints [2] and the behavior of tubular joints under cyclic loading [3–5]. Fillet welds, which are often used for their inexpensive cost and simple creation, are generally adopted in welded joints. This weld is vitally important to ensure the normal function of the joint. There are currently two design methods for fillet welds, the pre-qualified method and the fit-for-purpose method [6]. The pre-qualified method requires that the weld be proportioned to develop the yield strength of the connected branch wall at all locations around the branch. The design provision for a fillet weld, based solely on the thickness of the branch, is generally conservative and results in a relatively large weld size. The fit-for-purpose method requires that the weld be designed to resist the applied load in the branch. The design method takes the weld mechanical properties into consideration and results in an appropriate weld size.

When the applied axial load transfers from the branch to the chord in the tubular joints, the connection deformation caused by the flexibility of the connection must be considered. Therefore, the proper mode for load distribution in welds needs to be studied when the fit-for-purposed method is used to judge the strength of welds. Frater [7,8] and Packer [9] explored the strain distribution in welds for RHS joints through a series of experimental setups and proposed effective weld lengths. The AISC "Specification" [10] adopts the effective length and puts forward a weld design formula for RHS joints under axial tension. For tubular joints with CHS branches to SHS chord, nevertheless there are currently few research work (see Fig. 2). Thus axial tensile behavior testing and finite element analysis (FEA) are conducted in this paper to investigate the strain distribution, the failure modes and strength of welds for these type of joints.

2. Experimental program

2.1. Specimens

Eight X-joint specimens were tested, including five non-rigid joints and three rigid welded joints. The non-rigid joints referred to directly welded joints, varying in parameters included the width ratio β and the joint angle θ (see Fig. 3). The rigid joints were referred to butt joints with a stiffener plate. The square chord was replaced by the plate in rigid joints to eliminate flexible deformation of the welds, in

* Corresponding author.
E-mail address: weiwang@tongji.edu.cn (W. Wang).

http://dx.doi.org/10.1016/j.jcsr.2015.08.044
0143-974X/© 2015 Elsevier Ltd. All rights reserved.

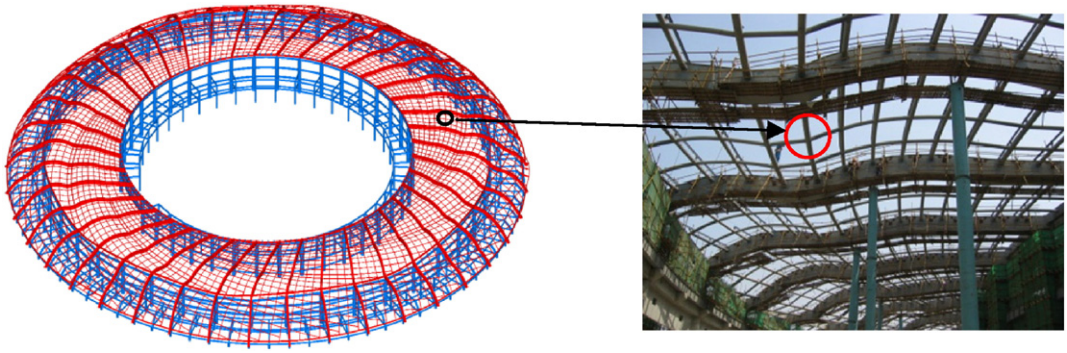

Fig. 1. Engineering application of tubular X-joints.

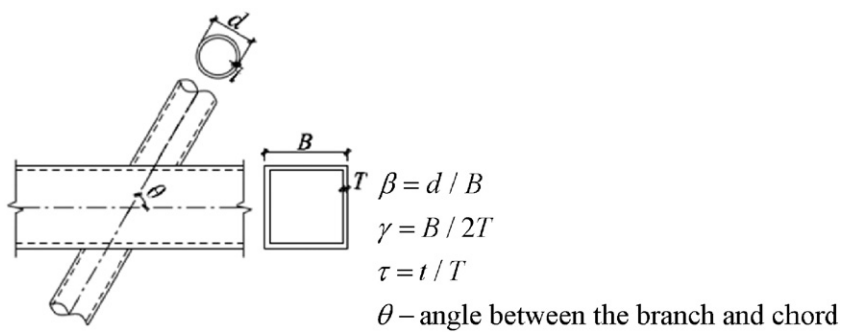

Fig. 2. X-joints with CHS branches to the SHS chord.

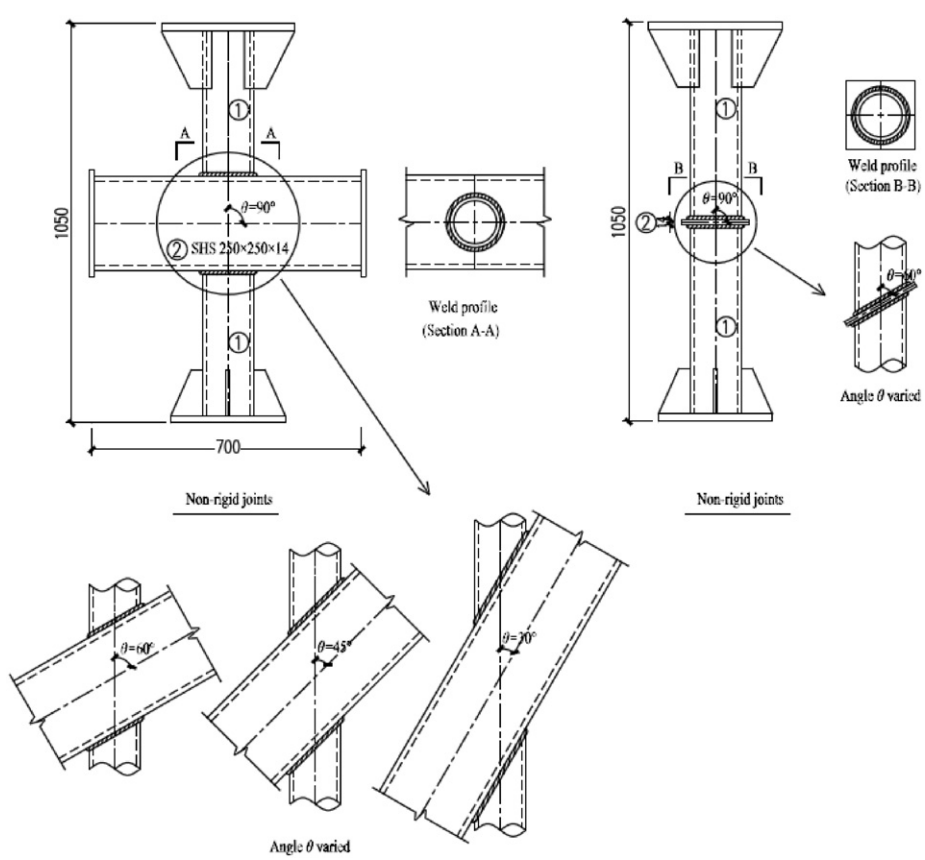

Fig. 3. Details of the specimens.

Table 1
Geometrical characteristics of the specimens.

Specimen	Section① (mm)	Section② (mm)	θ	β	Expected h_f (mm)
X90-1	CHS133 × 10	SHS250 × 250 × 14	90°	0.53	6
X90-2	CHS 180 × 10	SHS250 × 250 × 14	90°	0.72	6
X60-1	CHS 133 × 10	SHS250 × 250 × 14	60°	0.53	6
X45-1	CHS133 × 10	SHS250 × 250 × 14	45°	0.53	6
X30-1	CHS133 × 10	SHS250 × 250 × 14	30°	0.53	6
GX90-1	CHS133 × 10	−180 × 14	90°	0.53	6
GX90-2	CHS180 × 10	−230 × 14	90°	0.72	6
GX60-1	CHS133 × 10	−210 × 14	60°	0.53	6

Table 2
Measured material properties.

Sections	Material	f_y (MPa)	f_u (MPa)	f_y/f_u	Elongation (%)
CHS133 × 10	Q345B	348	529	0.66	26
CHS180 × 10	Q345B	375	563	0.67	27
SHS250 × 250 × 14	Q345B	325	401	0.81	24
Weld metal	E50 eletrode	416	500	0.83	27

comparison with the non-rigid joints. The details of the specimens are shown in Fig. 3. The properties of the specimens are shown in Table 1. When naming each specimen, 'X' or 'GX', respectively, refers to non-rigid or rigid joints and the number indicates the value of θ. The notation '−1' and '−2', respectively, corresponds to two different values of β. For all the specimens, the length of the branch was about three times greater than its diameter to allow the uniform load transmission from the branch to the connection region. Similarly, the length of the chord was about three times its width.

All the specimen members were fabricated from Q345B steel. Fillet welds were used for all X-joints in accordance with code GB50661-2011 [11]. Material characteristic testing for the steel and weld metal was carried out prior to the experiments [12]. The measured material properties are listed in Table 2.

Because the behavior of the welds was the main focus and the tests were meant to be weld-critical, the expected leg size (h_f) for each fillet weld, namely the leg length along the chord and the branch, was specified to be 6 mm based on pre-experimental analysis. To quantify the actual geometric properties of the welds, a silicone rubber impression was used to shape a negative mold of the welds in each specimen (see Fig. 4). The impression material was mixed first to shape the negative

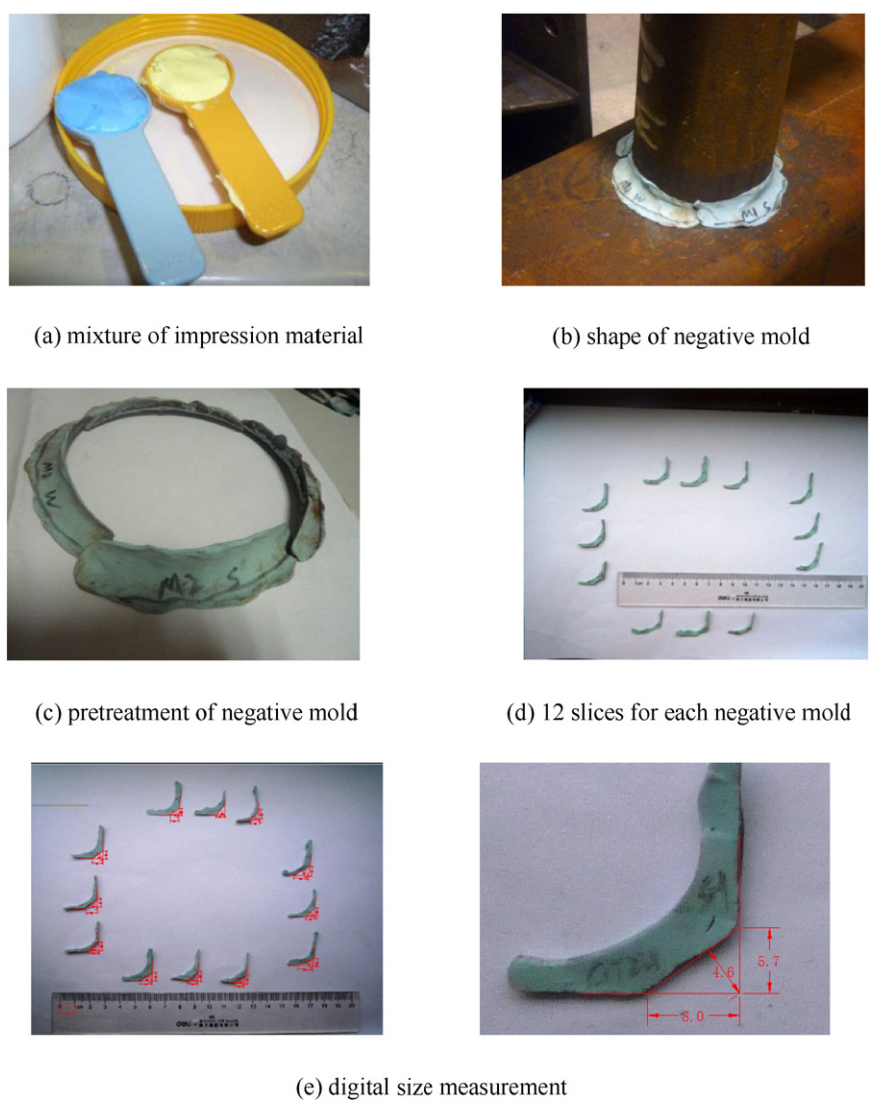

(a) mixture of impression material

(b) shape of negative mold

(c) pretreatment of negative mold

(d) 12 slices for each negative mold

(e) digital size measurement

Fig. 4. Measurement process for geometric properties of the welds using the negative mold method.

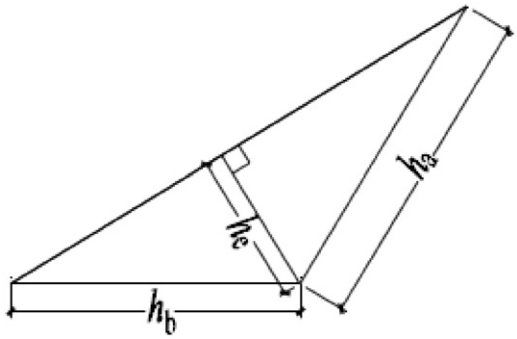

Fig. 5. Geometric properties of the welds.

Table 3
Measured average effective thickness h_e for each joint (in mm).

Specimen	X90-1	X90-2	X60-1	X45-1	X30-1	GX90-1	GX90-2	GX60-1
U	5.0	5.1	6.0	6.1	7.7	5.0	4.4	7.1
L	5.5	4.5	6.1	6.7	8.2	4.7	4.6	6.4

mold. Each mold was cut into 12 slices at specific locations along the intersection line to digitally measure the weld size. The leg length along the branch (h_a), the leg length along the chord (h_b) and the effective thickness (h_e) of each slice were measured (see Fig. 5). The average effective thickness for each joint is given in Table 3. The labels 'U' and 'L' stand for the upper part and the lower part of the X joints, respectively.

2.2. Test setup and loading procedure

A view of the testing arrangement is shown in Fig. 6 and the typical setup for the non-rigid and rigid joints is shown in Fig. 7. All the specimens were statically tested to failure by an axial tension loading applied in the branch. The main data derived from the testing included the relative deformation in the connection and the strain distribution in the welds around the intersection line. The strain distribution was measured using strain gauges secured to the branch approximately 15 mm from the weld toe to avoid any strain concentrations. The strain gauges were oriented in the direction of the branch and were used to record the strain in the welds. A typical test measurement arrangement is shown in Fig. 8.

3. Test results and discussion

3.1. Failure modes

For non-rigid joints, an initial crack was observed at the weld toe on the chord. The initial crack grew quickly to the nearby weld toe when the load increased before fracture occurred through the wall of the chord. For rigid joints, sudden fracture occurred at the connections when the load reached the maximum value.

The failure modes in the test included: (1) fracture in the wall of the chord along the weld toe (CF), (2) fracture of the weld metal (WF), and (3) fracture of the material in the heat affected zone of the branch (BHAZF). The different failure modes are shown in Fig. 9. Mode CF is generated when the material in the heat affected zone of the chord is unable to deform itself into the wall of the chord. This mode is observed in all the non-rigid joints. Mode WF occurs when the weld metal is incapable of transmitting the axial load, resulting in brittle rupture. Mode BHAZF occurs from weakness in the connection between the weld and the heat affected zone in the branch. Generally, modes WF and BHAZF are observed in rigid joints.

3.2. Load curves versus the relative deformation

Load curves versus the relative deformation for each specimen are shown in Fig. 10. The yield strength (P_{by}) and the ultimate strength (P_{bu}) for the cross section of the branch are clearly denoted in the figure. In addition, the ultimate deformation $\Delta_{Lu} = 0.03B$ [13] is also marked to study the deformation growth in the non-rigid joints. Significant deformation is observed in the non-rigid joints, indicating that the joints fail when the relative deformation is remarkable. The fracture of each non-rigid joint occurs when the relative deformation exceeds Δ_{Lu}, with the exception of specimen X90-2. For rigid joints, the specimens fail at very low deformations because there is no flexible deformation in the joints.

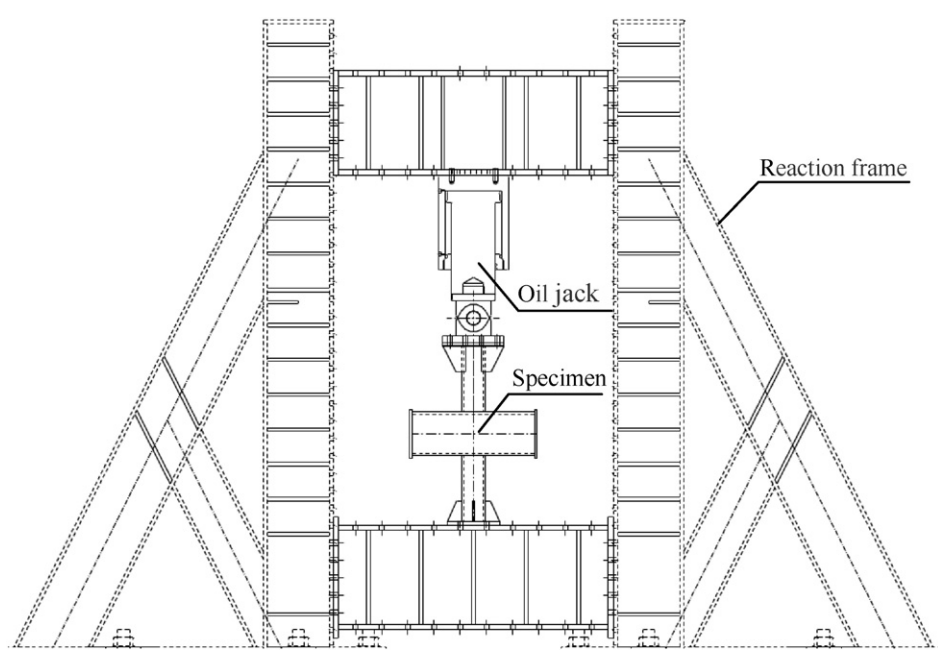

Fig. 6. Overview of the testing arrangement.

Fig. 7. Test setup.

3.3. Load curves versus the strain around the circumference

Load curves versus strain curves of the welds in the upper part of specimens X90-1 and GX90-1 are shown in Figs. 11 and 12, as representatives of non-rigid and rigid joints, respectively. The strain at measurement points 'a' and 'b' in the figures corresponds to the equivalent strain calculated by the strain rosette. The yield strain of the branch calculated using the measured material properties is also marked as ε_y. Fig. 12 shows that there is a uniform strain distribution in the rigid joints. However, the strain distribution is uneven in the non-rigid joints, as shown in Fig. 11. For welds at specific positions, such as measurement point '3', '4' and '5', there is dramatic strain growth. In contrast, the welds at other positions, such as measuring points '1' and '7', exhibit little strain growth.

The uneven strain distribution for the welds in non-rigid joints is related to the load transmission path. During load transmission, the applied load is first transmitted to the welds in the upper branch before being passed on to the top flange of the chord. Afterwards, the load flows from the flange to the web of the chord and finally to the lower branch (see Fig. 13). Welds at different positions around the intersection line play different roles during load transmission. Welds at positions close to the web of the chord bear a large proportion of the load during load transmission from the branch to the welds. This is a result of the sufficient boundary support provided by the nearby web of the chord. For local welds at positions far away from the web of the chord, the conclusion is the opposite and results in an uneven strain distribution.

3.4. Loading efficiency and effective length of the welds

Fig. 11 shows the load versus the strain distribution relationship for the welds in non-rigid joints. The difference in the strain growth indicates a discrepancy in the load transmission for local welds at different positions. The slope of the load-strain curve for each measurement

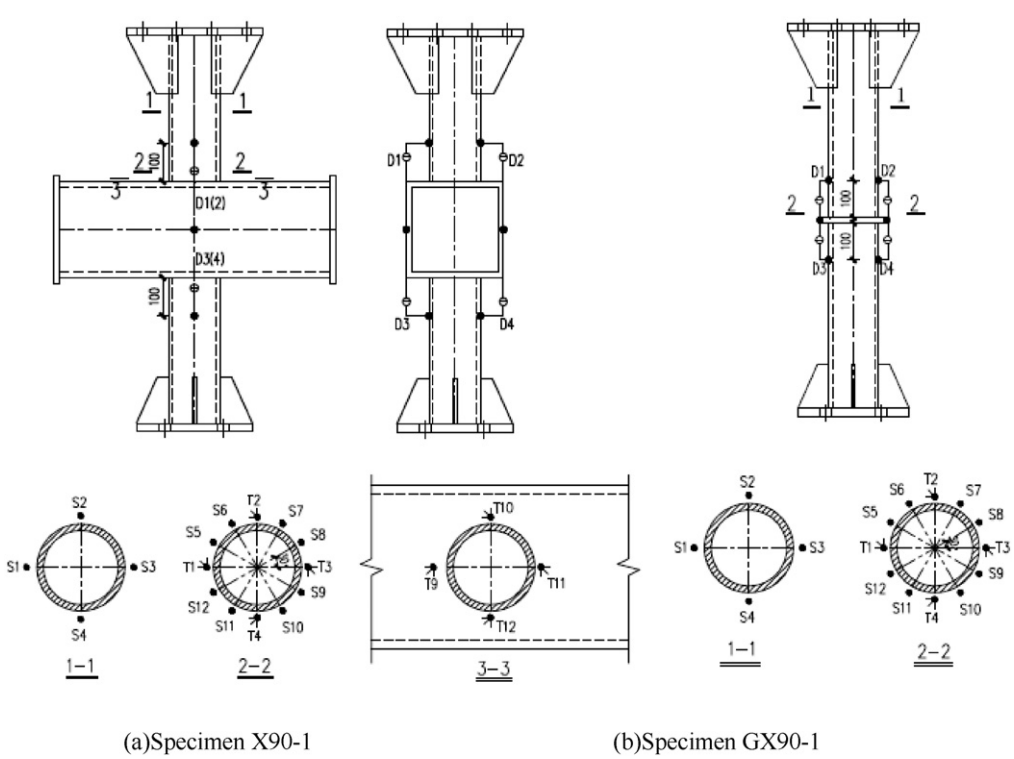

Fig. 8. Instrumentation arrangement.

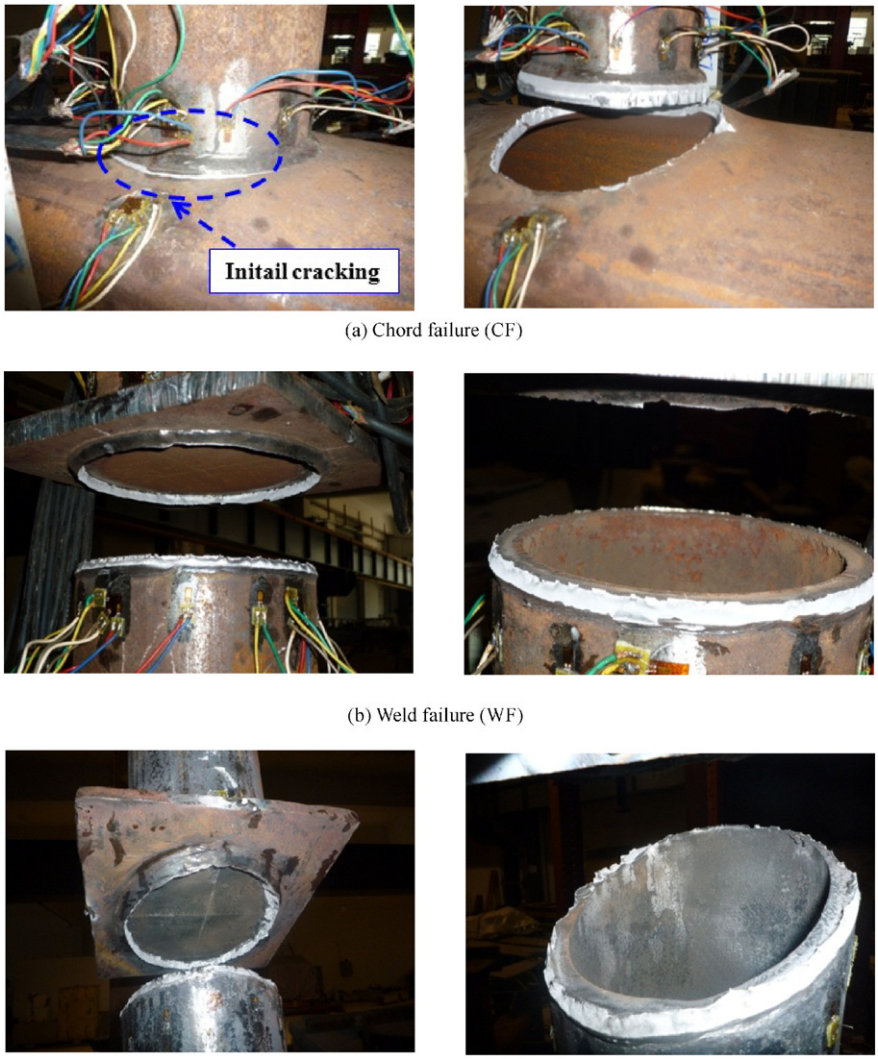

(a) Chord failure (CF)

(b) Weld failure (WF)

(c) Branch's HAZ failure (BHAZF)

Fig. 9. Failure modes of specimens.

point is first studied when the joint experiences elastic loading, which is marked as k_i. The minimum absolute value of the slope occurs at the measurement point with the quickest strain growth, which is marked as k_m. The local loading efficiency factor of the welds η is therefore defined to quantify the uneven strain distribution according to Eq. (1). Therefore, η is considered to provide a criterion to evaluate the strain growth, as well as the load distribution in the welds:

$$\eta = \frac{k_i}{k_m}. \tag{1}$$

As shown in Fig. 14, the generalized abscissa X is defined by the projection of the intersection line onto the axis of the chord. Therefore, the generalized abscissa value of the left and right endpoints of the intersection line is -1 and 1, respectively. The relationship between η and X (see Fig. 15) describes how the weld behaves during load transmission. The curves are shaped like mountains, with peaks at the center and decreases along both sides, corresponding to the law describing the load transmission path.

To examine the uneven load distribution, an effective length factor χ is defined by Eq. (2) according to the η–X curves:

$$\chi = \frac{\sum \eta dl}{L_w} \tag{2}$$

where dl is the length of a weld segment if the intersection line is divided into several parts and calculated from mathematical characteristics and L_w is the geometric length of the intersection line. Those segments containing negative values for η are excluded. The effective length factors computed from the experimental results are shown in Table 4. Therefore, the uneven weld load distribution around the intersection line is equivalent to the uniform distribution along the effective length of χL_w.

3.5. Axial tensile strength prediction of the welds

The analysis of the axial strength of the welds for all the joints is listed in Table 5. Most joints failed suddenly, with the fracture occurring through the weld metal and/or base metal. The variable P_{max} refers to the maximum axial load in the test. The symbol '>' in the table refers to a situation in which the joint has a strength that is potentially greater than the P_{max} given in the table because the joint was unable to load to fracture. This was because of the limitations of the test equipment. The yield strength (P_{by}) and the ultimate strength (P_{bu}) of the branch are listed in the table. The plastic capacity of the chord (P_{ju}) and the punching capacity of the chord (P_{su}) with reference to the ISO 14346 "recommendations" [14] are also included in the table. The variable P_{max} is always lower than P_{bu}, eliminating the possibility of fracture in

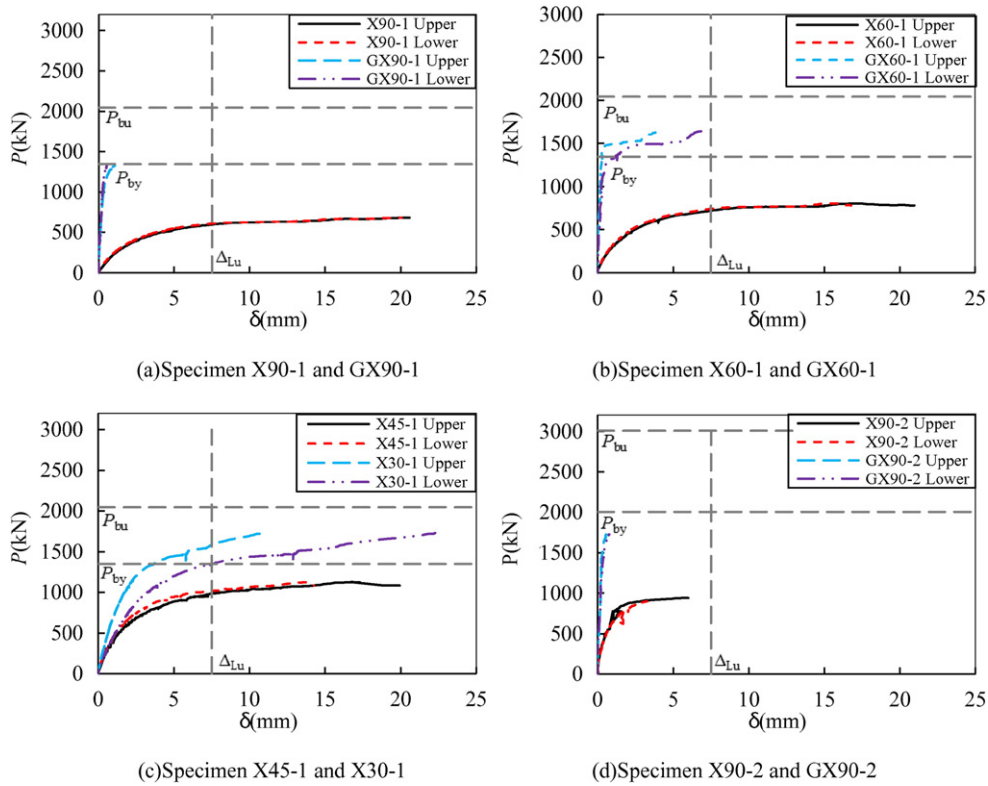

(a)Specimen X90-1 and GX90-1

(b)Specimen X60-1 and GX60-1

(c)Specimen X45-1 and X30-1

(d)Specimen X90-2 and GX90-2

Fig. 10.. Load versus relative deformation curves.

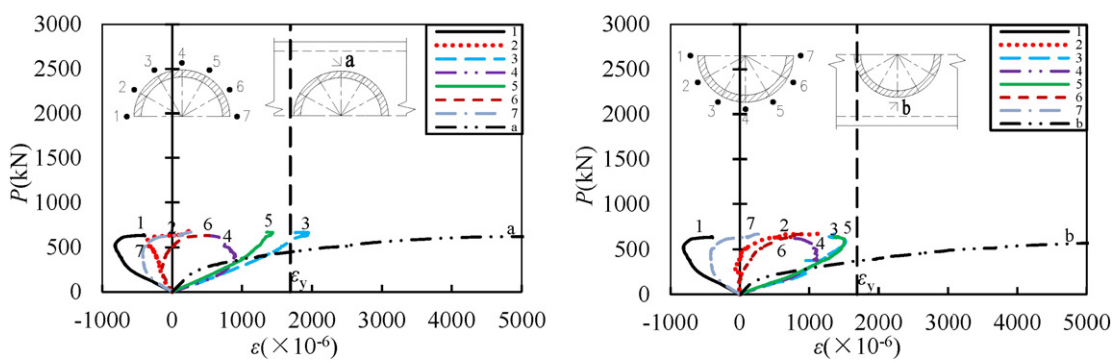

(a) Load versus strain curves for X90-1(I)

(b) Load versus strain curves for X90-1(II)

Fig. 11. Load versus strain curves around the circumference for the upper part of specimen X90-1.

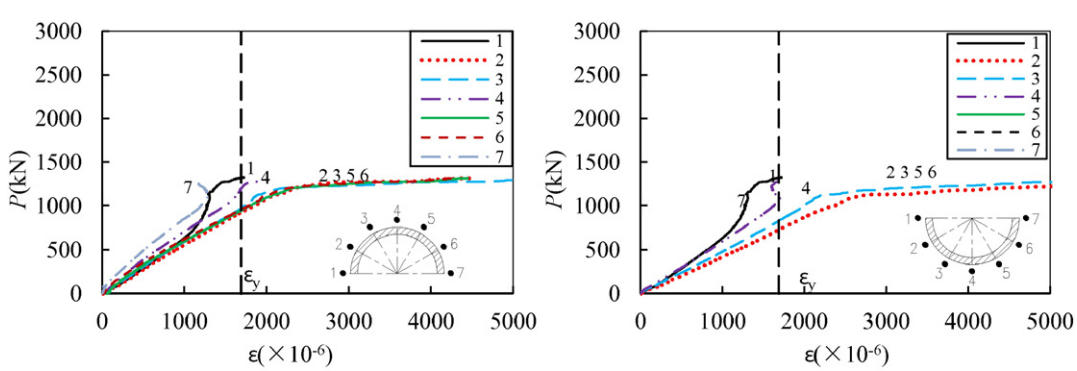

(a) Load versus strain curves for GX90-1(I)

(b) Load versus strain curves for GX90-1(II)

Fig. 12. Load versus strain curves around the circumference for the upper part of specimen GX90-1.

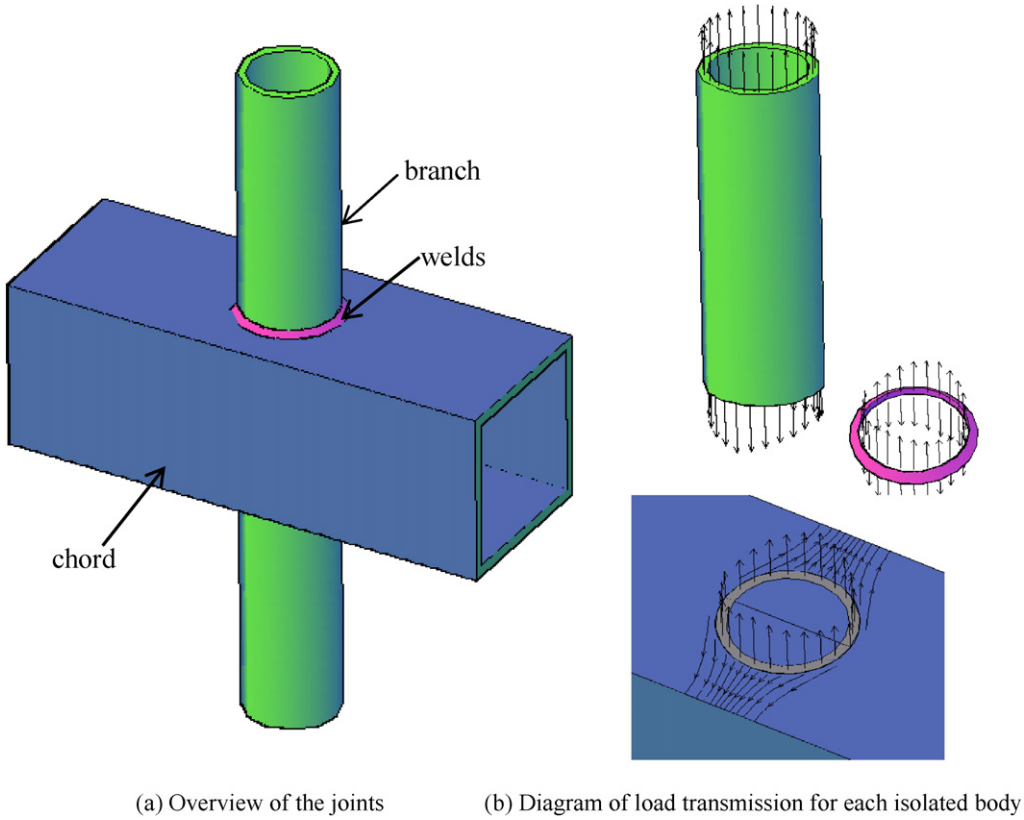

Fig. 13. Load transmission in the non-rigid joints.

the branch. At the same time, P_{max} is less than P_{su}, which is greater than P_{ju} for non-rigid joints. This validates that the main failure mode for non-rigid joints is CF due to the fracture of the heat affected zone of the chord.

It is noted that failure in all the joints includes the fracture of the weld metal and the material in the heat affected zone. For the former, the fracture load reflects the mechanical behavior of the weld itself. For the latter, the ultimate strength of the welds needs to be higher than the maximum axial load for the test because the heat affected zone fails before the weld. Nevertheless, P_{max} is considered to be the ultimate strength for the welds regardless of the distinction mentioned above, which is indicative of a certain degree of safety when predicting the strength of welds.

4. Finite element analysis of the axial tensile behavior of the welds

4.1. Finite element models and verification

The finite element analysis was performed with the ANSYS software package involving geometrical nonlinearity. The finite element models were established according to the geometric characteristics of each non-rigid joint and the measured material properties summarized in Table 2 as the FEA multi-linear material model. The SOLID95 element was selected as the element type and a hexahedral mesh was used for the finite element model. In addition, a gap was placed between the branch and the chord because they are connected only by the fillet weld around the intersection line in reality. The weld and the finite element model are shown in Fig. 16.

The comparison of the load versus relative deformation curves between the experiment and the FEA is shown in Fig. 17. The experimental and FEA curves are in good agreement in terms of the initial stiffness. Differences are shown to appear when the relative deformation

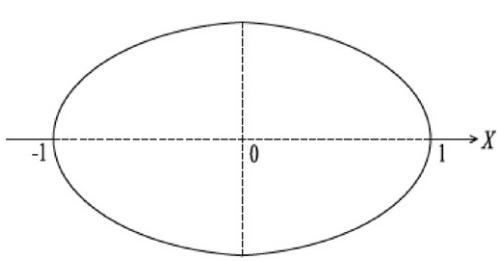

Fig. 14. Diagram of the generalized abscissa X.

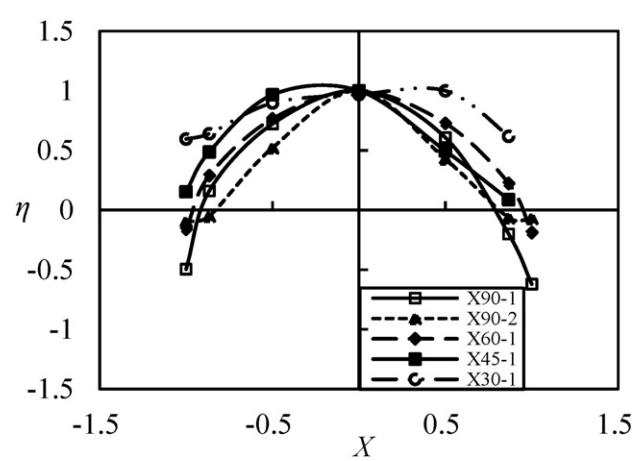

Fig. 15. The local loading efficiency factor for the welds around the intersection line for the non-rigid joints.

Table 4
The effective length factor χ for welds in non-rigid joints.

Specimen	X90-1	X90-2	X60-1	X45-1	X30-1
Computed by experimental results	0.385	0.316	0.458	0.458	0.583
Computed by the fitting formula	0.372	0.353	0.420	0.500	0.670

Table 5
Analysis of the weld strength.

Specimen	P_{ju} (kN)	P_{su} (kN)	P_{by} (kN)	P_{bu} (kN)	P_{max} (kN)	Failure mode
X90-1	406	860	1345	2044	684	CF
X90-2	635	1164	2003	3007	945	CF
X60-1	489	1092	1345	2044	806	CF
X45-1	641	1539	1345	2044	1125	CF
X30-1	1040	2823	1345	2044	>1729	CF
GX90-1	/	/	1345	2044	1323	WF
GX90-2	/	/	2003	3007	>1727	Not fail
GX60-1	/	/	1345	2044	1644	WF, BHAZF

grows. This may be due to difficulties associated with accurately simulating the size and material properties of the weld, as well as neglecting the crack mechanism in the finite element analysis. As the loading efficiency and the effective length of the welds during the elastic stage is the main focus of this research, the finite element analysis is still employed to simulate the experiment and may be utilized for further parameter analysis.

4.2. Parametric analysis of the effective length factor

To study the effective length factor during general conditions for non-rigid joints, a parameter analysis was performed using the finite element method. The parameters include θ, β, τ and γ, which are varied over the common range listed in Table 6. An elastic analysis was carried out over a total of 144 finite element models.

During the finite element analysis, the stress distribution in the wall of the branch approximately 15 mm from the weld toe was considered to replace the distribution in the welds. The local loading efficiency factor may be calculated using Eq. (3):

$$\eta = \sigma_i/\sigma_{max} \tag{3}$$

where σ_i is the axial stress along the branch at the previously mentioned positions in the joint and σ_{max} is the maximum σ_i at the different positions in the joint.

The η–X curves for several joints are shown in Fig. 18. We may conclude that the parameters γ and θ have a great influence on the shape of the curve. The reason for this assertion is that the parameter γ reflects the stiffness of the chord, whereas parameter θ affects the length and the features of the intersection line.

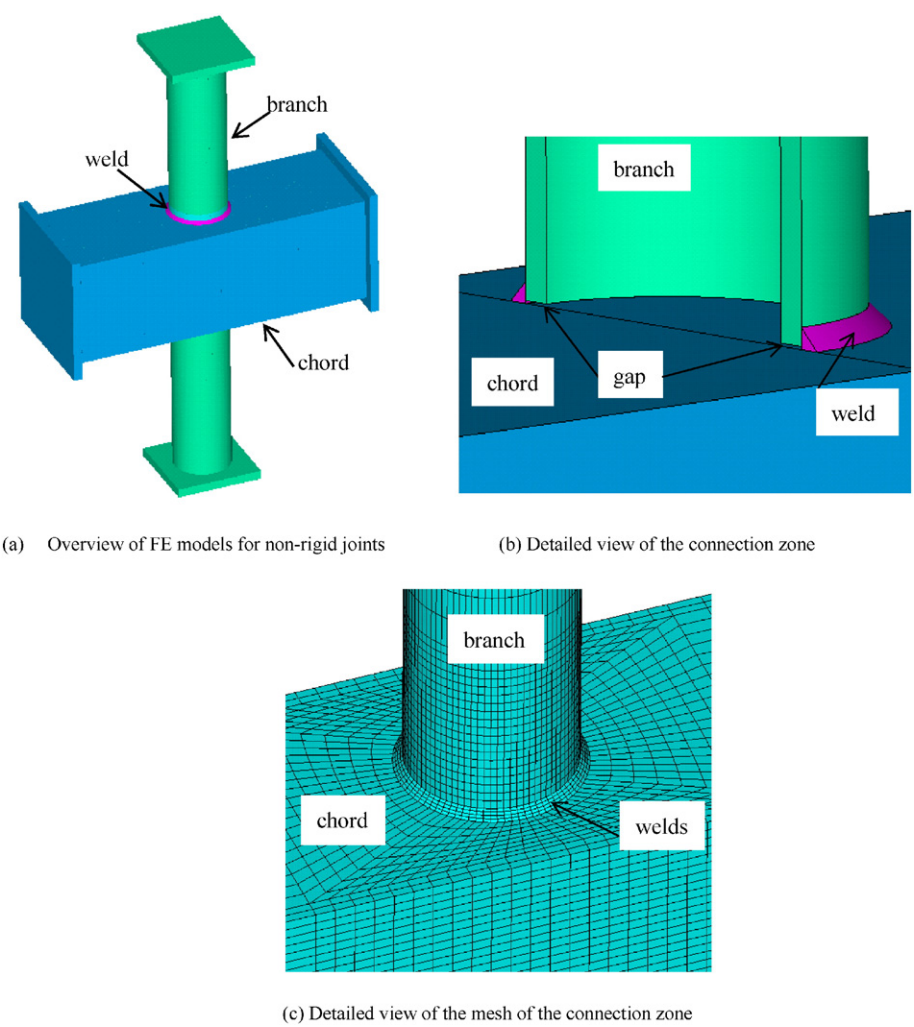

(a) Overview of FE models for non-rigid joints

(b) Detailed view of the connection zone

(c) Detailed view of the mesh of the connection zone

Fig. 16. Finite element model and weld configuration.

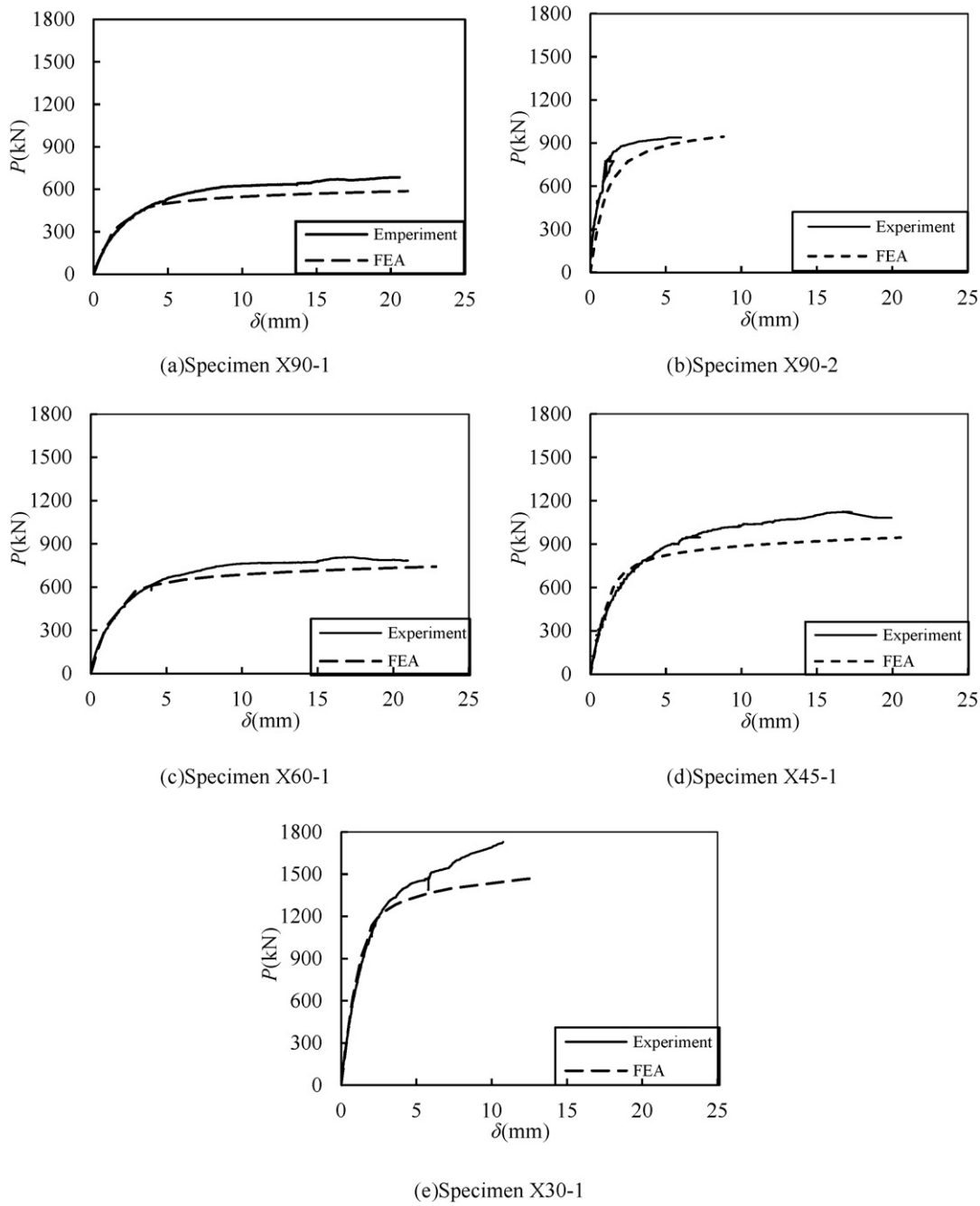

Fig. 17. Comparison of load versus relative deformation curves between the experiment and the FEA.

Based on Eq. (2), the result of the effective length factor for the 144 finite element models was studied and a fitting formula for χ was proposed in Eq. (4):

$$\chi = \frac{1.61}{(\sin\theta)^{0.85}} \cdot \frac{1}{3.05+\beta} \cdot \frac{1}{(\gamma - 4.61)^{0.13}} \tag{4}$$

Table 6
Parameters of the joints.

θ	β	τ	γ
90°	0.4	0.4	5
60°	0.6	0.7	10
45°	0.8	1	20
30°			30

The comparison of the value of χ computed from the experimental results and the fitting formula is listed in Table 4, and exhibits good agreement.

5. Strength prediction of welds and safety assessment

In the AISC "Specification" [10], the design strength ϕR_n ($\phi = 0.75$) for welded joints shall be the lower value of the base material strength determined according to the limit states of the tensile and shear rupture and the weld metal strength determined according to the limit state of rupture as follows.

For the base metal:

$$R_n = F_{nBM} A_{BM} \tag{5}$$

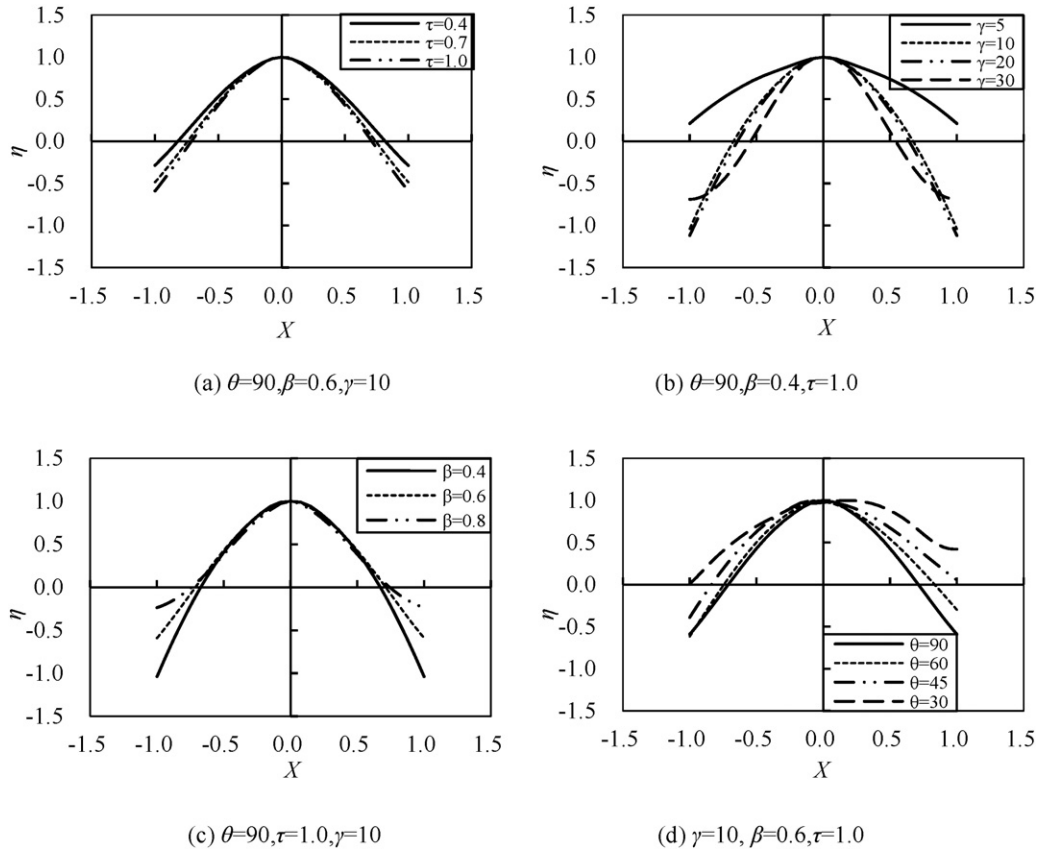

(a) θ=90,β=0.6,γ=10 (b) θ=90,β=0.4,τ=1.0

(c) θ=90,τ=1.0,γ=10 (d) γ=10, β=0.6,τ=1.0

Fig. 18. The η–X curves for joints of various parameters.

where F_{nBM} is the nominal stress of the base metal and A_{BM} is the cross-sectional area of the base metal.

For the weld metal:

$$R_n = F_{nw}A_{we} = F_{nw}h_eL_w \tag{6}$$

$$F_{nw} = 0.6F_{EXX} \tag{7}$$

where F_{nw} is the nominal stress of the weld, A_{we} is the effective area of the weld and F_{EXX} is the ultimate stress of the weld metal.

The "Specification" notes that the nominal stress of the weld F_{nw} can be adjusted by a strength enhancement factor of $(1 + 0.5\sin^{1.5}\theta)$ using the following formula for a linear weld group with a uniform leg size:

$$F_{nw} = 0.6F_{EXX}\left(1 + 0.5\sin^{1.5}\theta\right) \tag{8}$$

where θ is the angle of loading measured from the weld longitudinal axis.

The experimental results show that the main failure mode in the non-rigid specimens is chord failure in the wall along the weld toe, instead of rupture in the cross-section of the base metal. Thus, the predicted strength of the welds may be calculated using Eq. (6) based on the weld metal strength. As the "Specification" does not explicitly indicate

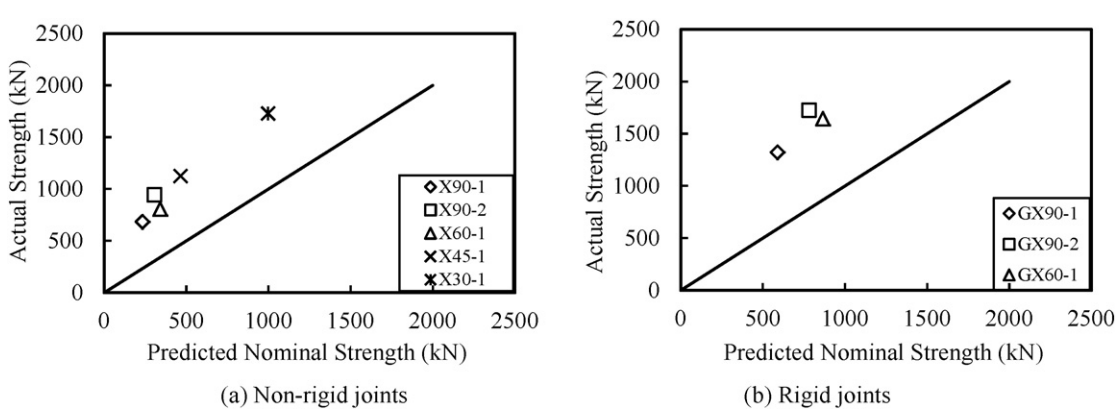

(a) Non-rigid joints (b) Rigid joints

Fig. 19. Actual strength versus predicted strength for welds without the inclusion of the enhancement factor $(1 + 0.5\sin^{1.5}\theta)$.

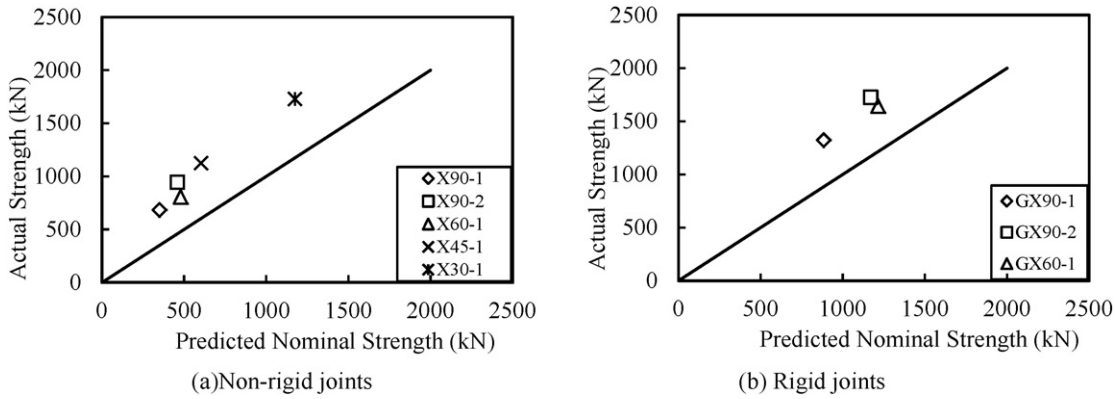

Fig. 20. Actual strength versus predicted strength for welds when including the enhancement factor $(1 + 0.5\sin^{1.5}\theta)$.

that the strength enhancement of the weld described in Eq. (8) is permitted for welds in tubular joints, two methods to determine the predicted strength of the weld based on Eqs. (7) and (8) are used to make the comparison. The effective length factor χ is used to replace the geometric length of the welds L_w with the effective length χL_w. Therefore the predicted strength of welds for non-rigid joints R_n^j can be determined from:

$$R_n^j = F_{nw} \times h_e \times \chi L_w \tag{9}$$

For rigid joints, the geometric length of the welds L_w is retained due to the uniform strain distribution in the welds. The predicted strength of the welds may therefore be determined using Eq. (6).

The measured geometric and mechanical properties of the welds are used herein to evaluate the predicted weld strength. The maximum axial load for each joint is considered to be the actual weld strength. The predicted strength versus the actual strength of the welds without or with the inclusion of the enhancement factor $(1 + 0.5\sin^{1.5}\theta)$ is shown in Figs. 19 and 20. The actual strength always exceeds the predicted strength, demonstrating the safety of the predicted formula.

To assess the safety margins of the predicted strength of the welds, a reliability safety index of β^+ with a commonly assigned value of 4.5 is checked using a simplified reliability analysis in which the resistance factor ϕ is given by the following equation specified in [15]:

$$\phi = m_R \exp(-\alpha\beta^+ \mathrm{cov}) \tag{10}$$

where m_R is the mean of the ratio of the actual strength to the predicted strength of the welds, cov is the coefficient of variation of this ratio, and α is coefficient of separation, which is taken to be 0.55 [16].

Solving Eq. (10) yields values of $\phi = 1.56$ for non-rigid joints and $\phi = 1.77$ for rigid joints when the strength enhancement factor $(1 + 0.5\sin^{1.5}\theta)$ is not considered. When the strength enhancement factor is considered, $\phi = 1.36$ for non-rigid joints and $\phi = 1.29$ for rigid joints. Because all the values of ϕ exceed 0.75, which is specified by the AISC LRFD method, the predicted formula is deemed to be safe and meets the requirement for the resistance factor. When the strength enhancement factor is taken to determine the strength of the welds on the basis of the available experimental evidence, the predicted strength of the weld is still deemed to be conservative.

6. Conclusions

Based on experiments performed using eight X-type specimens, the strain distributions, failure modes and strengths of the welds were studied. The conclusions that can be drawn from this work are as follows:

(1) The axial strength of the welds in non-rigid joints is much lower than those in the corresponding rigid joints. This is the result of an uneven loading distribution in the non-rigid joints, as well as fracture of the material in the heat affected zone due to its brittleness.

(2) The local loading efficiency factor curves η versus the generalized abscissa X for the welds are shaped similarly to mountains with peaks at the center and decreases along both sides, corresponding to the law describing the load transmission path.

(3) The formula for predicting the strength of the welds according to the effective length is proposed and proven to meet the reliability requirement for the AISC LRFD method.

It is noted that the resistance factor ϕ induced by the predicted formula is conservative to some extent, which indicates that the predicted weld strength may require corrections from other aspects other than the loading efficiency mechanism. Therefore, further study is required when enough test data becomes available.

Acknowledgments

The research presented in this paper was supported by the Natural Science Foundation of China (NSFC) through Grant No. 51378380. Any opinions, findings, conclusions, and recommendations expressed in this paper are those of the authors and do not necessarily reflect the views of the sponsors.

References

[1] W. Wang, Y.Y. Chen, Modelling and classification of tubular joint rigidity and its effect on the global response of CHS lattice girders, Struct. Eng. Mech. 21 (6) (2005) 677–698.
[2] Y.Y. Chen, W. Wang, Flexural behavior and resistance of uni-planar KK and X tubular joints, Steel Compos. Struct. 3 (2) (2003) 123–140.
[3] W. Wang, Y.Y. Chen, B.D. Zhao, Effects of loading patterns on seismic behavior of CHS KK-connections under out-of-plane bending, J. Constr. Steel Res. 73 (2012) 55–65.
[4] W. Wang, Y.Y. Chen, X.D. Meng, R.T. Leon, Behavior of thick-walled CHS X-joints under cyclic out-of-plane bending, J. Constr. Steel Res. 66 (6) (2010) 826–834.
[5] W. Wang, Y.Y. Chen, Hysteretic behaviour of tubular joints under cyclic loading, J. Constr. Steel Res. 63 (10) (2007) 1384–1395.
[6] M.R. McFadden, J.A. Packer, Weld design and fabrication for RHS connections, Steel Constr. 6 (1) (2013) 5–10.
[7] G.S. Frater, J.A. Packer, Weldment design for RHS truss connections. I: applications, J. Struct. Eng. ASCE 118 (10) (1992) 2784–2803.
[8] G.S. Frater, J.A. Packer, Weldment design for RHS truss connections. II: experimentation, J. Struct. Eng. ASCE 118 (10) (1992) 2804–2819.
[9] J.A. Packer, C.E. Cassidy, Effective weld length for HSS T, Y, and X connections, J. Struct. Eng. ASCE 121 (10) (1995) 1402–1408.
[10] American Institute of Steel Construction, Specification for Structural Steel BuildingsChicago, USA 2010.
[11] GB50661-2011, Code for Welding of Steel Structure, China Architecture &Building Press, Beijing, 2011.
[12] Y.Y. Chen, W. Sun, T.M. Chan, Cyclic stress–strain behavior of structural steel with yield strength up to 460 N/mm^2, Front. Struct. Civ. Eng. 8 (2) (2014) 178–186.

[13] L.H. Lu, G.D. De Winkel, Y. Yu, J. Wardenier, Deformation limit for the ultimate strength of hollow section joints, 6th International Symposium on Tubular Structures 1994, pp. 341–347.
[14] ISO 14346, Static Design Procedure For Welded Hollow-Section Joints — Recommendations, International Organization for Standardization, Switzerland, 2013.
[15] J.W. Fisher, T.V. Galambos, G.L. Kulak, M.K. Ravindra, Load andresistance factor design criteria for connectors, J. Struct. Div. ASCE 104 (9) (1978) 1427–1441.
[16] M.K. Ravindra, T.V. Galambos, Load and resistance factor design for steel, J. Struct. Div. ASCE 104 (9) (1978) 1337–1353.